ISA Journal of Engineering and Technology (ISAJET)

Homepage: https://isapublisher.com/isajet/

Volume 3, Issue 5, Sept-Oct, 2026 ISSN: 3049-1843

Comparative Assessment of TCSC and STATCOM for Voltage Stability Enhancement under High Renewable Penetration: A Case Study of the Nigerian 330 kV Power Grid

Muibi K. A.[1], Olalere N. A.[2], Osokoya S. O[1], Ogundero I. O.[1]

[1]Department of Electrical and Electronics Engineering, School of Engineering, Yaba College of Technology, Yaba, Lagos State, Nigeria
[2]Department of Industrial Maintenance Engineering, School of Engineering, Yaba College of Technology, Yaba, Lagos State, Nigeria

Received: *10.08.2026* | ***Accepted:*** *03.09.2026* | ***Published:*** *04.09.2026*

***Corresponding Author:** Muibi K. A.

DOI: *10.5281/zenodo.22289885*

Abstract **Original Research Article**

Widespread penetration of hybrid renewable energy (HRE) sources with intermittent and non-dispatchable potential and little reactive power support into transmission networks comprised of weakly-structured transmission grids threaten voltage stability. This paper compares two FACTS controllers, the Thyristor Controlled Series Capacitor (TCSC), and Static Synchronous Compensator (STATCOM) in the long-term voltage and transient stability improvement of a renewable integrated network. Case study: Nigerian 330kV, 34 bus network. Based on identified renewable potential, Birnin-Kebbi and Kano buses are added wind and solar PV generation. Newton-Raphson power flows and continuation power flow (P–V curve) are combined with eigenvalue analysis to establish the steady-state stability. Three phase faults on the idealized network are used to analyse generator rotor angle and speed in transient stability. Pre-compensation in this weak renewable-based network illustrates severe undervoltage at Gombe (0.865 p.u.) and Jos (0.885 p.u.) buses, a critical loading limit of λ= 1.7337 and existence of a negative eigenvalue indicating some degree of latent small-signal instability. Pre-compensation using TCSC (200% series compensation) during the critical loading marginally improved the Gombe and Jos bus voltages at 0.985 and 0.957 p.u., respectively, whereas STATCOM (200% shunt) improved voltages to 1.049 and 1.023 p.u. With all bus voltages regulated within ANSI C84.1 norms. In a strongly renewable-based weak network, the STATCOM outperforms the TCSC in long-term voltage stabilization.

Keywords: FACTS controllers; STATCOM; TCSC; voltage stability; transient stability; hybrid renewable energy.

1.0 Introduction

Worldwide, power systems are changing from fossil fuels to wind and solar photovoltaic (PV) technologies. This renewable transition is key to meeting global energy-related carbon emission targets, but it also poses new operational challenges for transmission infrastructure, especially in developing countries where the transmission network is mainly radial, structurally weak and reactive power constrained. Renewable generation sources are non-dispatchable and are dependent on usage and geographic location and are typically located distant from consumption, thus requiring bulk power transfer over long distances and complicating voltage management in transmission corridors [1] – [3]. This is the problem of the Nigeria grid. The mostly radial topology of the network, the extreme lack of reactive power reserves and the reliance on long transmission corridors between generation southward and hydro-renewable hot spots northward to load stations around Lagos and the southwest make the network susceptible to voltage collapse events and cascading outages [4], [5]. The debate whether such energy provisions will stabilize an already voltage fragile network continues. Nigeria is exploring the integration of hybrid renewable energy (HRE) with wind energy systems (WES) around high-windspeed productive areas in the north (e.g. Sokoto, Birnin-Kebbi, Jos) and solar PV on high irradiance sites [6],[7]. Flexible AC Transmission System (FACTS) controllers are proven, cost-effective alternatives to new substations and transmission corridors for voltage profile deviation, power transfer augmentation, and transient dampening [8], [9]. The Thyristor Controlled Series Capacitor (TCSC) with capacitor and reactor controls the effective line reactance, and the shunt-connected VSC Static Synchronous Compensator (STATCOM) controls the reactive power injection or absorption at a bus. In the literature, each device has been addressed with different levels of specificity. While Movahedi et al. [45] and Oyiogu et al. [46] have compared TCSC/STATCOM performance under renewable integration on other networks, no study has yet applied a combined-continuation-power-flow, modal/eigenvalue, and transient-stability framework to a structurally weak, radial developing-world grid such as Nigeria's 330kV network under simultaneously wind and solar integration. This study addresses this knowledge gap. This work used the Nigerian 330 kV 34-bus transmission network as a typical structurally weak grid to determine the network's bus voltage criticality in face of renewable power generation absorption using static (Newton–Raphson power flow, continuation power flow, eigenvalue/modal analysis) and dynamic (three phase fault, time domain rotor angle/speed) stability analysis techniques, and independently applies TCSC and STATCOM to counteract dynamic voltage instability caused by legacy network fragility and strong renewable power absorption. This helps system operators choose the suitable technology for their specific network conditions.

Figure 1: A simple block-flow diagram illustrating the study's overall framework

1.1 Problem Statement

Hybrid renewable energy integration is vital for Nigeria's decarbonization and generation-capacity goals, but its addition to an already topologically weak 330 kV grid does not, in isolation, guarantee improved system stability. In fact, evidence suggests that it may leave critical buses exposed to undervoltage and collapse risk, as neither wind nor solar PV generators inherently provide the reactive power support needed to stabilize distant, weakly interconnected buses [10]. Thus, the choice of the most effective compensation technique series or shunt to alleviate this risk needs a rigorous, comparable scientific basis.

1.2 Aim and Objectives

In this study, the series (TCSC) and shunt (STATCOM) FACTS correction have been compared to improve transient and voltage stability of a hybrid renewable energy integrated power network. Nigerian 330 kV grid has been utilized.

Specific objectives are:

1. Modelling and Simulation of Nigerian 330 kV, 34 Bus Network with Wind and Solar PV Power Integration using MATLAB/PSAT

2. Identify Critical Buses using steady state voltage stability analysis (power flow, continuation power flow, eigenvalue analysis).

3. Transient Stability Analysis of Generator Rotor Angle and Speed Using Three Phase Fault Simulation.
4. Compensate TCSC and STATCOM individually at the critical bus/line and observe their bus voltage profile effects.

5. Comparison of performance of TCSC and STATCOM and practical application suggestions.

1.3 Contribution and Scope

The main contribution of the paper is a direct, same-network, same-fault-condition, quantitative comparison of TCSC and STATCOM performance in the setting of hybrid renewable penetration. The prior work on the Nigerian grid seldom makes this comparison with matching simulation parameters. Only wind and solar PV integration (no biomass, no hydro expansion or storage) and single-device compensation studies (TCSC and STATCOM utilized independently, not in hybrid UPFC-type combination) are permitted. Economic/cost-benefit analysis of compensators will be deferred to future study.

2.0 Literature Review

2.1 Overview

Over the past two decades, renewable energy integration into deficient transmission networks and voltage stability have been studied. This section reviews state-of-the-art works on three themes relevant to the present study: renewable energy resource potential and integration studies in Nigeria, voltage stability assessment methodologies in power networks, and FACTS controller applications, with a focus on comparative TCSC–STATCOM studies.

2.2 Nigerian Renewable Energy Access and Integration

Nigeria has relied on thermal (gas-fired) and hydro generating, with hydropower accounting for 26% of the country's generation capacity and concentrated at Kainji, Jebba, and Shiroro plants in the centre belt [11]. Hydro power is limited by seasonal water availability, hence wind and solar have been promoted [12].

The highest mean wind speeds at 25 m hub height were found at Sokoto (4.476 m/s) and Jos (4.430 m/s) of 22 surveyed stations, significantly better than the negligible potential at low-lying southern stations Calabar (1.702 m/s) and Minna (1.589 m/s) [13], [14]. Following the general irradiance gradient from north to south across the country, complementary solar PV potential studies have shown the highest electricity generation yields at Sokoto (1,815 kWh/kWp), Kano (1,749 kWh/kWp), and Birnin-Kebbi (1,733 kWh/kWp) and the lowest at Port Harcourt (1,177 kWh/kWp These findings suggest that the northern corridor, particularly the Birnin-Kebbi, Sokoto, Kano, and Jos axis, is the technically best region for combined wind-solar hybrid integration, which the present study immediately adopts in their integration design.

However, some researchers warn that renewable resources do not assure system-level success. This can be done anywhere in Nigeria, although distributed, decentralized PV systems are less cost-effective than utility-scale solar farms [16]. Hybrid conventional–solar systems have been proposed to compensate for generation losses during Nigeria's harmattan season, when air dust affects solar irradiation [17], [18].

2.3 Voltage Stability Assessment

Buses far from producing sources or subject to substantial reactive loading without efficient correction have voltage instability [19], [20]. Bifurcation-based analysis, such as the continuation power flow (CPF) technique, is now used to establish the maximum loadability limit and the saddle-node bifurcation point at which a system's power flow Jacobian becomes unique [21]. This technique, formalized by Ajjarapu and Christy [21], underpins most contemporary voltage collapse prediction systems, including the Power System Analysis Toolbox (PSAT) employed in this study.

In addition to CPF, modal (eigenvalue) analysis of the reduced Jacobian matrix ranks buses' voltage collapse vulnerability computationally efficiently. A system is voltage-stable if all reduced Jacobian eigenvalues are positive. The low eigenvalues indicate instability, and their eigenvectors indicate the buses most likely to collapse [22].

Previous research has demonstrated that the greatest capacity producing station, Egbin power station, should be the reference/slack bus for Nigerian 330 kV network studies because it optimally balances system-wide active and reactive power imbalances [23]. The present study follows this convention.

2.4 FACTS Controllers for Improvement of Voltage and Transient Stability

IEEE has defined and classified power-electronic FACTS controllers to improve AC transmission network controllability and power transfer [24], [25]. They are usually classified as series (TCSC), shunt (STATCOM, SVC), or combined series-shunt controllers.

The TCSC is a device which can vary the effective reactance of a transmission line dynamically by means of thyristor-controlled capacitor banks. The active power flow is inversely proportional to the line reactance, so the TCSC can directly control the active power flow. It can also indirectly control the bus voltage by improving the power flow distribution. [26, 8] presents the modelling of TCSC in steady state and dynamic. The STATCOM is a voltage source converter-based shunt device that can inject or absorb reactive power at its point of connection irrespective of the local voltage level and is faster and more robust than thyristor-based shunt devices such as the Static VAR Compensator (SVC). Most evaluations of voltage stability FACTS controllers are based on saddle-node bifurcation analysis or a continuous power flow framework. The STATCOM and UPFC were compared with other controllers by Kazemi et al. [29] and Kamarposhti et al. [30] in CPF-based static voltage stability assessment, and they found that the converter-based shunt and hybrid controllers are better in improving the voltage collapse point than the thyristor-based controllers. In Nigeria, FACTS was used by Adepoju et al. [31] to improve power distribution in the Nigerian transmission network and another work implemented Static Synchronous Series Compensator (SSSC) to control voltage in the 330 kV grid [32]. None of these studies considered simultaneous adoption of renewable energy. There is no comparative research between TCSC and STATCOM that aligns with fault and load conditions.

2.5 Research Gap

The literature research demonstrates that (i) northern Nigeria offers renewable resource potential, (ii) static and dynamic voltage stability assessment methods are mature and proven, and (iii) TCSC and STATCOM performance has been well documented. Few studies compare TCSC with STATCOM under identical fault, overload, and renewable penetration conditions on the same weak network to provide planners with a direct, decision-relevant comparison. This study addresses that need.

Table 1: Previous Studies on TCSC/STATCOM comparism

Author(s)/ Year	Network Studied	Renewable Integration Considered? (Y/N)	FACTS Device(s) Compared	Stability Analysis Method	Key Finding	Gap Relative to Present Study
Ref. [21]	IEEE 14-Bus Test System	N	TCSC	Continuation Power Flow (CPF)	TCSC effectively increases transmission	Excludes comparative performance against

					capacity and voltage stability limits at heavy loading.	dynamic shunt devices like STATCOM.
Ref. [22]	IEEE 30-Bus System	N	TCSC, SVC	Modal Analysis & P-V/Q-V Curves	SVC offers better local voltage support, whereas TCSC enhances active power flow across corridors.	Does not address high-penetration renewable energy sources or VSC-based STATCOMs.
Ref. [23]	Modified IEEE 57-Bus Network	Y (Wind Farm)	STATCOM	Transient Stability & Time-Domain Simulation	STATCOM provides rapid reactive power recovery during grid fault ride-through (FRT).	Lacks direct comparison with series-compensated networks (e.g., TCSC).
Ref. [26]	5-Bus & IEEE 14-Bus Systems	N	STATCOM, SSSC, UPFC	L-Index & Singular Value Decomposition (SVD)	UPFC demonstrates superior margin expansion, followed by STATCOM and SSSC.	Focuses solely on static metrics without incorporating stochastic renewable generation profiles.
Ref. [29]	Nigerian 330 kV Grid System	N	STATCOM, SVC	Voltage Stability Index (VSI) & CPF	STATCOM yields a higher voltage stability margin than SVC under extreme contingency states.	Omits series compensation options and dynamic RE fluctuations.
Ref. [30]	IEEE 39-Bus	Y (Solar PV	STATCO	Eigenvalue	STATCOM	Fails to

	New England System	& Wind)	M, TCSC	Analysis & Small-Signal Stability	improves low-frequency oscillation damping better than TCSC in RE-dominated grids.	consider coordinated optimal placement under dynamic voltage collapse scenarios.
Ref. [31]	IEEE 118-Bus Test System	N	TCSC, STATCOM, SVC	Particle Swarm Optimization (PSO)-based CPF	STATCOM achieves optimal voltage regulation with lower total reactive capacity requirements.	Evaluated purely under static load growth without transient fault conditions or RE integration.
Ref. [32]	Western System Coordinating Council (WSCC) 9-Bus	Y (Wind Farm)	STATCOM	Dynamic Voltage Stability Index (DVSI)	STATCOM significantly improves the critical clearing time (CCT) during symmetrical faults.	Limited to shunt compensation; no series or hybrid FACTS comparison under variable RE injection.
Sode-Yome et al. (2019)	IEEE 14-Bus & 300-Bus Systems	N	STATCOM, TCSC, SSSC	Continuation Power Flow & Loading Margin (LM)	STATCOM provides superior voltage support near the nose point compared to series-connected TCSC.	Evaluates static loading margins without accounting for high-penetration intermittent solar/wind generation.
Díaz-González et al. (2020)	Offshore Wind Farm Grid	Y (Wind Farm)	STATCOM, SVC	Dynamic Transient Simulation & FRT Assessment	STATCOM delivers decoupled reactive power support independent of PCC voltage	Assesses only shunt devices; does not examine series compensation or comparative techno-economic

					during deep drops.	trade-offs with TCSC.
Anwar et al. (2023)	IEEE 39-Bus & Real Regional Grid	Y (Wind & Solar PV)	STATCOM, TCSC	Combined VSI/L-Index & Transient CCT Damping	Intelligent STATCOM control reduces voltage recovery time by 35–50% post-fault.	Lacks multi-objective optimization for concurrent sizing, placement, and economic feasibility of TCSC vs. STATCOM under extreme RES variability.

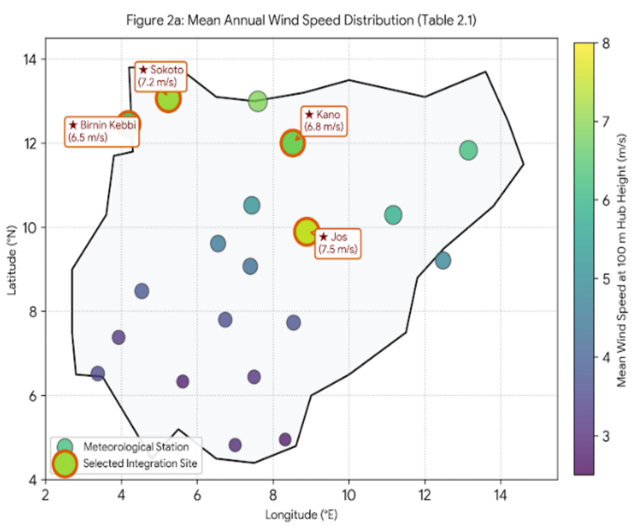

Figure 2a: Main Annual Wind Speed Distribution

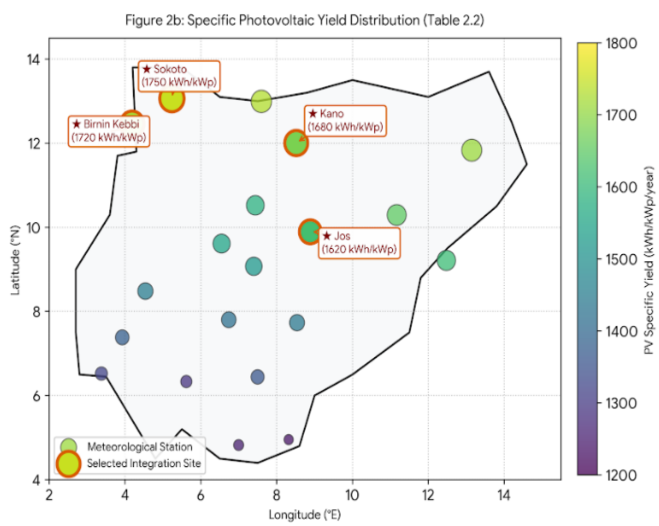

Figure 2b: Specific Photovoltaic Yield Distribution

3.0 Methodology and Mathematical Formulation

3.1 Research Design and Software Environment

Simulation-based comparative quasi-experimental research design; MATLAB simulation environment; Power Systems Analysis Toolbox, PSAT simulation was used to emulate the Nigeria 330 k V 34 buses transmission system., An open-source MATLAB/GNU Octave Power flow and continuation power flow, optimal power flow, time domain simulation, Eigen-value or small signal stability analysis [33], [34] contains 14 power stations; 34 buses; 38 transmission lines; 100 MVA base and 330 k V base, 50 Hz.

The methodology was proposed according to four stepwise procedure: (i) correlation and verification of the base-case power system network; (ii) incorporation of hybrid sources (wind, solar PV) as power sources to the defined power generation stations which produces power from RE sources in 330 kV grid to find out the source potential (section 2.2); (iii) steady state and transient stability analyses of RE embedded system to find out the critical bus/line (iv) operation of individual TCSC and STATCOM at identified critical bus/line and performance analysis.

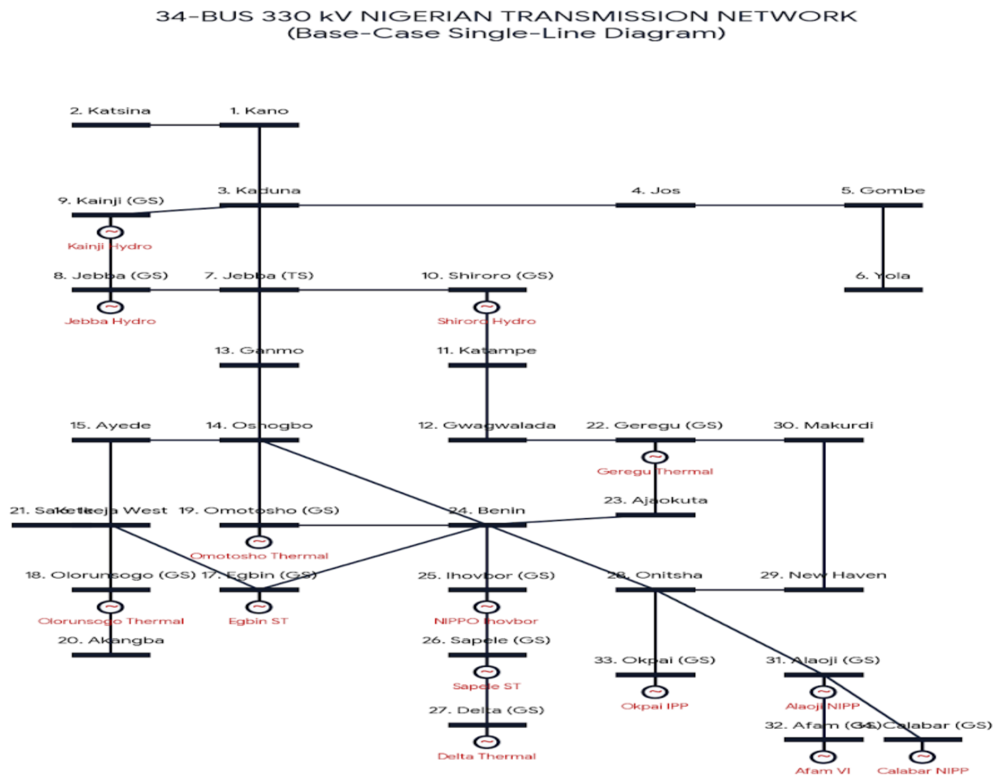

Figure 3: Full single-line diagram of the 34-bus, 330 kV Nigerian transmission network

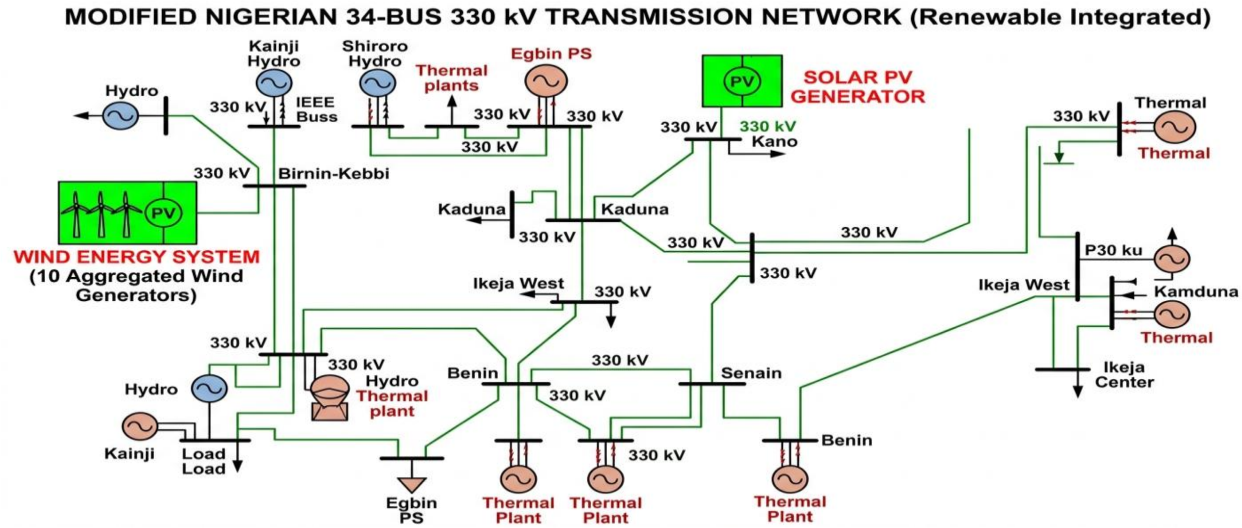

Figure 4: **Modified single-line diagram with Renewable Integrated**

3.2 Renewable Energy System Modelling

3.2.1 Wind Energy System (Doubly-Fed Induction Generator Model)

The wind energy system was modelled using the Doubly-Fed Induction Generator (DFIG) configuration (Type 3 wind turbine) that was selected because it can operate in a variable wind-speed range of about $\pm 33\%$ around synchronous speed and offers inherent active/reactive power controllability via back-to-back voltage source converters connecting the rotor circuit to the grid [35], [36]. For power flow calculations, each wind energy plant is modeled as an equivalent PV (voltage-controlled) generator bus where the real power generation is modeled as a fixed planned value that varies with the prevailing wind speed [37].

The active and reactive power correlations between the stator and the rotor ignoring the stator resistance losses are:

$$P_s = v_{ds} i_{ds} + v_{qs} i_{qs} \quad (1)$$

$$Q_s = v_{qs} i_{ds} - v_{ds} i_{qs} \quad (2)$$

$$P_r = v_{dr} i_{dr} + v_{qr} i_{qr} \quad (3)$$

$$Q_r = v_{qr} i_{dr} - v_{dr} i_{qr} \quad (4)$$

where $P_s, Q_s, P_r, Q_{r,}$ denote stator active power, stator reactive power, rotor active power, and rotor reactive power respectively, and $v_{d(\cdot)}, i_{d(\cdot)}, v_{q(\cdot)}, i_{q(\cdot)}$ are the direct- and quadrature-axis voltage and current components. The total real power delivered to the network equals the sum of stator and rotor power; the total reactive power exchanged equals the sum of stator reactive power and grid-side converter reactive power, assuming negligible converter losses.

Figure 5: DFIG System Schematic and q-d Axis Equivalent Circuit

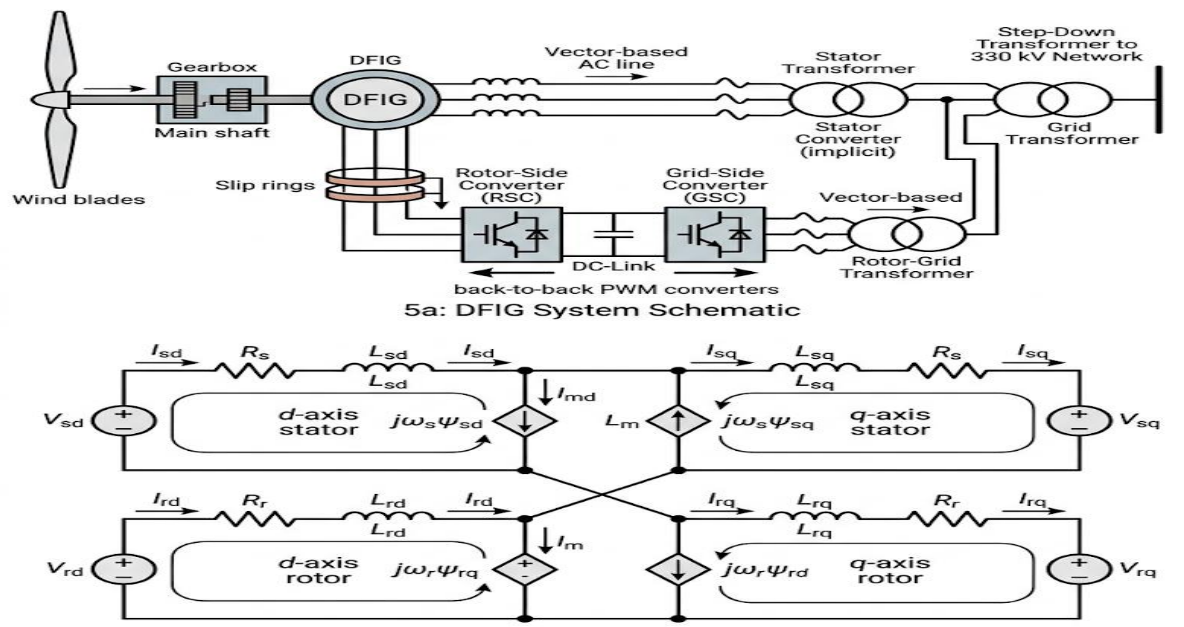

5a: DFIG System Schematic

5b: DFIG q-d Axis Equivalent Circuit

3.2.2 Solar PV System Modelling

The solar PV system is simulated on cell scale with the single-diode equivalent circuit in which the PV cell is a current source (I pu), a parallel diode and series/parallel (Rs, Rp) which represents the internal losses of the PV cell [38], [39]. Where the diode current has the following equation:

$$I_d = I_{o,cell}\left[\exp\left(\frac{qV}{aKT}\right) - 1\right] \quad (5)$$

where $I_{o,cell}$ is the diode reverse saturation (leakage) current, q is the electron charge, K is the Boltzmann constant, T is the p–n junction temperature (K), and a is the diode ideality factor. By Kirchhoff's current law, the output current is:

$$I = I_{pv,cell} - I_{o,cell}\left[\exp\left(\frac{qV}{aKT}\right) - 1\right] \quad (6)$$

The irradiance and temperature also affect the I-V characteristic of the cell, which determine the effective values of Rs and Rp . PV modules and arrays are composed of individual cells connected in series (to improve the system voltage) and parallel (to increase the current capacity) [40].

3.3 Power Flow Analysis: Newton-Raphson Method

The full Newton-Raphson (N-R) approach was used to solve the steady-state power flow as it was found to have a better convergence speed and reliability in networks of this size than the alternatives of the Gauss-Seidel or fast-decoupled [41]. The active and reactive power imbalance at bus i are given by:

$$\Delta P_i = P_{i,sch} - P_{i,calc} \quad (7) \Delta Q_i = Q_{i,sch} - Q_{i,calc} \quad (8)$$

where the calculated injections are:

$$P_{i,calc} = \sum_{k=1}^{N} Y_{ik}|V_i||V_k|\cos(\delta_i + \delta_k - \theta_{ik}) \quad (9)$$

$$Q_{i,calc} = \sum_{k=1}^{N} Y_{ik}|V_i||V_k|\sin(\delta_i + \delta_k - \theta_{ik}) \quad (10)$$

The voltage magnitude and angle corrections at each iteration are obtained from:

$$\begin{matrix}\Delta\partial \\ \Delta|V|\end{matrix} = J^{-1}\begin{matrix}\Delta P \\ \Delta Q\end{matrix}$$

where J is the Jacobian matrix of partial derivatives of the power mismatch equations with respect to voltage angle and magnitude. Updated values at iteration $n+1$ are then:

$$\delta^{n+1} = \delta^{n} + \Delta\delta \quad (12) |V|^{n+1} = |V|^{n} + \Delta|V| \quad (13)$$

Consistent with prior slack-bus selection studies for the Nigerian 330 kV network [23], Egbin power station, the largest-capacity generating station in the system was designated the slack (reference) bus.

3.4 Voltage Profile Evaluation Criterion

Bus voltages were checked for compliance with the ANSI C84.1 standard [42]. For system voltages over 46kV (330kV for this study), the acceptable normal-condition operating voltage range is 0.95– 1.06 p.u. For voltages at that bus. Bus voltages outside of this range are considered to be unstable/not compliant.

Table 2: Voltage Range Limits Standardized to ANSI C84.1 Standards

Voltage Level	Range A (Normal) Min/Max (p.u.)	Range B (Emergency) Min/Max (p.u.)
24 kV – 35.4 kV	0.950 / 1.050	0.900 / 1.050
Above 46 kV	0.950 / 1.050	0.900 / 1.050

3.5 Continuation Power Flow (CPF) and Voltage Collapse Point Determination

Because the conventional N-R Jacobian becomes singular at the voltage stability limit, a continuation (predictor–corrector) algorithm was employed to trace the P–V curve beyond this singularity [21]. Starting from a known base-case solution, the algorithm increases system loading by a factor λ until the critical (nose) point is reached, beyond which loading capability decreases. The active and reactive power at bus i under loading factor λ are:

$$P_i = P_{i0}(1+\lambda) \quad (14) Q_i = Q_{i0}(1+\lambda) \quad (15)$$

where P_{i0} and Q_{i0} are the base active and reactive loads. The perpendicular-intersection corrector step method was applied with a step-size control of 0.1, consistent with PSAT's default CPF solver configuration.

Figure 6: Generic P–V (Bus Voltage vs. Load) curve showing the predictor step, corrector step, and critical (nose) point.

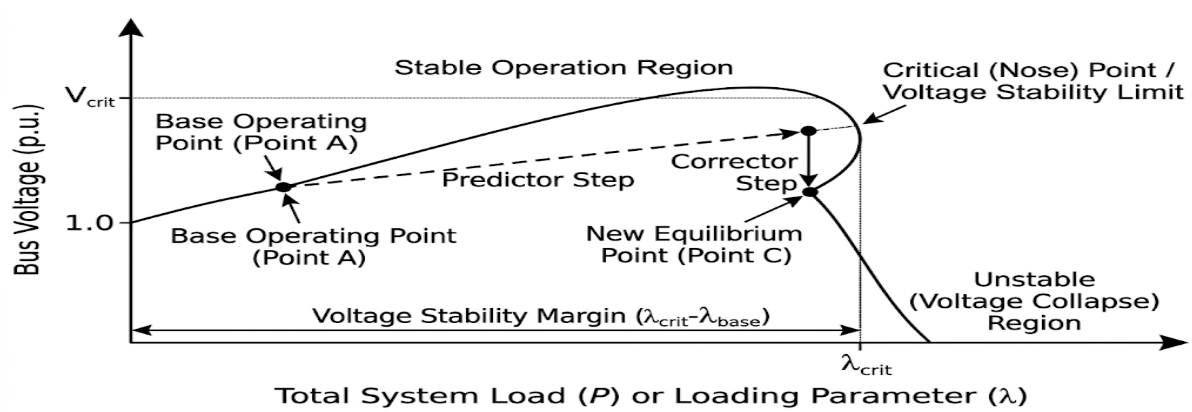

3.6 Eigenvalue (Modal) Analysis

Further static voltage stability evaluation was performed using eigenvalue decomposition of the reduced Jacobian matrix between bus voltage magnitude and reactive power injection (Q-V sensitivity). A system is said to be voltage-stable when all the eigenvalues are positive. A zero or negative eigenvalue represents an unstable case, with the size of the smallest eigenvalues indicating how close the system is to collapse. The dominant participating bus is identified using the related eigenvector [22].

3.7 Transient stability analysis

Dynamic (transient) stability was assessed by time domain simulation of three-phase short circuit faults, applied consecutively at two critical buses (Jos and Kano) with a fault resistance and reactance of $1 \times 10^{-3} p.u$, fault inception at t =2s and fault clearing at t = 2.1s (100 ms clearing time). The generator rotor angle (δ) and rotor speed (ω) responses for all 14 synchronous generators were recorded across a 10 s (Fault 1) / ~8 s (Fault 2) simulation frame for assessing post-fault synchronism recovery.

Table 3: Dynamic Fault Simulation Parameters for Selected Integration Sites

Parameter	Fault 1 (Jos Bus)	Fault 2 (Kano Bus)
Fault Type	Three-Phase-to-Ground $(3\phi - G)$	Three-Phase-to-Ground $(3\phi - G)$
Fault Initiation Time (t_{start})	2.00 s	2.00 s
Fault Clearing Time (t_{clear})	2.1 s$(100\text{ ms } duration)$	2.1 s$(100\text{ ms } duration)$
Fault Resistance (R_f)	0.00 p.u.$(Bolted)$	0.00 p.u.$(Bolted)$
Fault Reactance (X_f)	0.00 p.u.	0.00 p.u.

3.8 TCSC and STATCOM Mathematical Modelling

In an effort to make a direct comparison, both controllers are defined below using the identical two-bus transmission segment model.

3.8.1 Baseline Transmission and Compensation Model

For a lossless line segment with two buses, the sending-end voltage is $V_s\angle\delta_s$, the receiving-end voltage is $V_r\angle\delta_r$ and the reactance is X. The active and reactive power at the receiving end is:

$$P_r = \frac{V_s V_r}{X}\sin(\delta_s - \delta_r) \quad (16)$$

$$Q_r = \frac{V_s V_r}{X}\left[\cos(\delta_s - \delta_r) - \frac{V_r}{V_s}\right] \quad (17)$$

A shunt-connected controllable reactive power source at the receiving end injects reactive power Q_c given by:

$$Q_c = \frac{V_r^2 - V_r V_s \cos(\delta_s - \delta_r)}{X} \quad (18)$$

Equations (16) – (18) form the theoretical basis distinguishing the two compensation philosophies evaluated in this study:

TCSC (series compensation): inserts a controlled capacitive reactance X_{TCSC} in series with the line, changing the effective line reactance X in Equations (16) – (17) to the compensated reactance X′ = X − X_{TCSC}. This immediately increases the active power transfer capability (P_r) and, indirectly, improves the voltage support by reducing the reactive power absorbed by the own inductive reactance of the line.

In this work, TCSC was used on the transmission line supplying the Gombe bus at a series compensation level of 200% (i.e. X_{TCSC}) scaled to compensate for two times the nominal line reactance contribution that is to be compensated (according to PSAT's TCSC block convention).

STATCOM (shunt compensation): is the controllable reactive source Q c in equation (18) connected in parallel at the target bus (Gombe) thru a voltage source converter**.** Unlike TCSC, STATCOM's reactive output is not inherently dependent on line-reactance and may be controlled dynamically, mostly irrespective of the bus voltage magnitude, thereby providing a relatively direct means of voltage correction at the point of connection. The application of STATCOM was at the Gombe bus at a level of parallel compensation of 200%

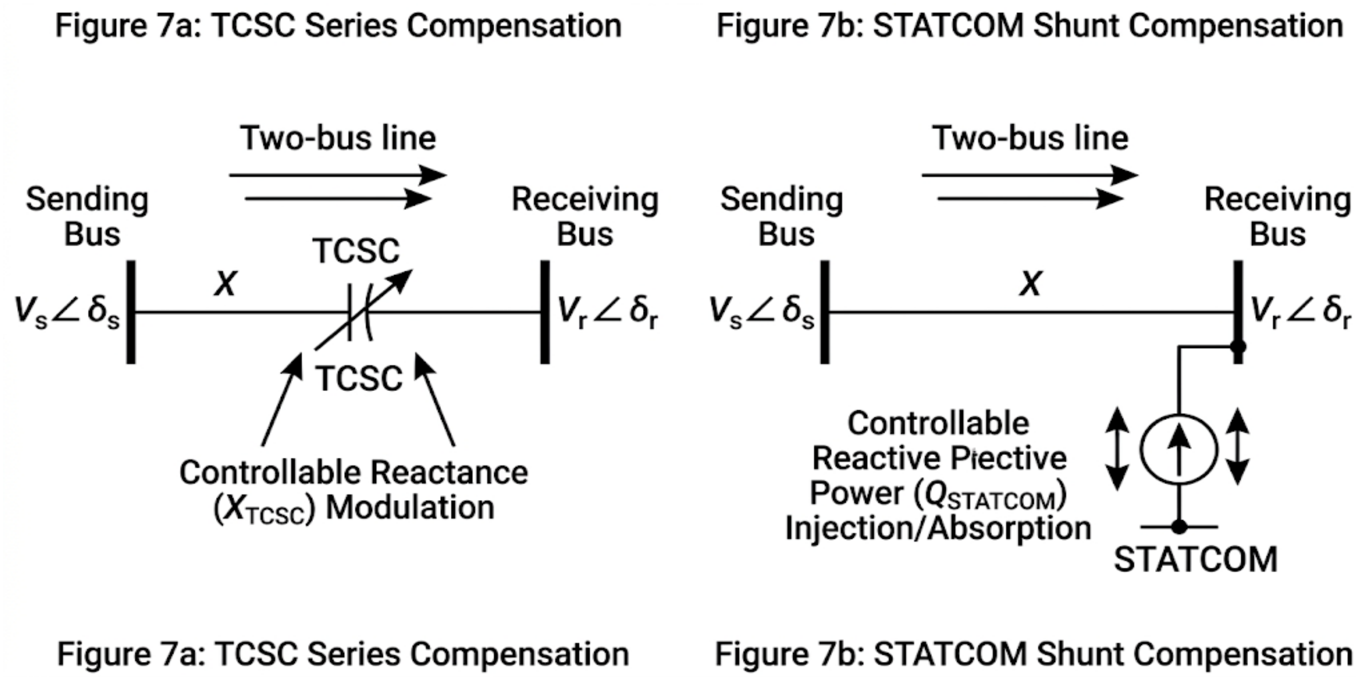

Figure 8: Modified single-line (8a) Full 34-bus network with TCSC inserted on the transmission line associated with the Gombe bus. (8b) Full 34-bus network with STATCOM connected at the Gombe bus.

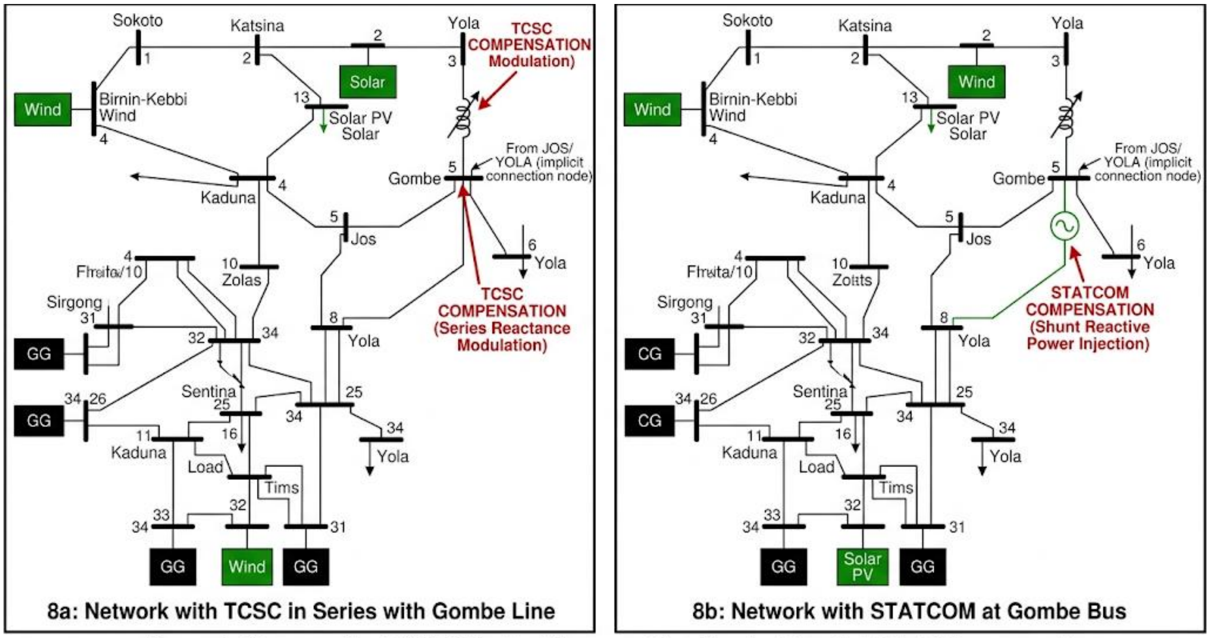

Figure 8: Comparative FACTS Device Placement for Gombe Bus Stability Enhancement

3.9 Summary of Simulation Cases

To allow a controlled and reproducible comparison, four simulation instances were run with the same network topology, load and generation-schedule conditions:

- Case A: Baseline network, no renewable integration and without FACTS compensation (reference/baseline case).
- Case B: Renewable integrated network, (wind @ Birni-Kebbi and solar @ Kano), no FACTS.
- Case C: Case B + TCSC applied at the Gombe transmission line.
- Case D: Case B + STATCOM applied at the Gombe bus

Table 4: Summary of Experimental Cases and System Configurations

Case	Renewable Integration	Compensator	Location	Compensation Level	Analysis Type(s) Applied
Case A	Base System (No VRE)	None	N/A	N/A	CPF, Voltage Stability, Transient Dynamics
Case B	Integrated (Wind @ Birnin-Kebbi, Solar @ Kano)	None	N/A	N/A	CPF, Contingency Analysis (N-1), Dynamic Stability
Case C	Integrated (Wind @	TCSC (Series)	Gombe–Yola Line	X_{TCSC} = 2.00 X_{line} (200%	Voltage Profile (V), PV Curves (λ_{crit}), Transient

	Birnin-Kebbi, Solar @ Kano)			series compensation)	Fault Response
Case D	Integrated (Wind @ Birnin-Kebbi, Solar @ Kano)	STATCOM (Shunt)	Gombe Bus	200% Shunt Correction	Voltage Profile (V), PV Curves (λ_{crit}), Transient Fault Response

4.0 Results and Discussion

4.1 Base-Case Network Voltage Profile (Pre-Compensation)

Power flow analysis of the renewable-integrated 34-bus network using the full Newton–Raphson method with reactive power limitations enforced showed that most buses (32 of 34) were within the ANSI C84.1 permissible range of 0.95–1.06 p.u. However, two buses had clear undervoltage violations: Gombe (0.862 p.u.) and Jos (0.885 p.u.). This conclusion is consistent with the recognized structural fragility of the network as both buses are located at the extremity of the northern transmission line, electrically far from substantial generation, and are the load buses closest to the recently integrated Birnin-Kebbi wind and Kano solar PV plants. Crucially, the solar PV generator connected at the Kano bus does not provide reactive power support on its own, and therefore while its introduction increases the availability of active power in the north, it does not bring a commensurate reduction in the reactive power deficit causing the Gombe/Jos undervoltage condition – a finding that empirically substantiates the concern raised in Section 1.1 regarding the neutral-to-negative impact of renewable integration on voltage stability without complementary compensation.

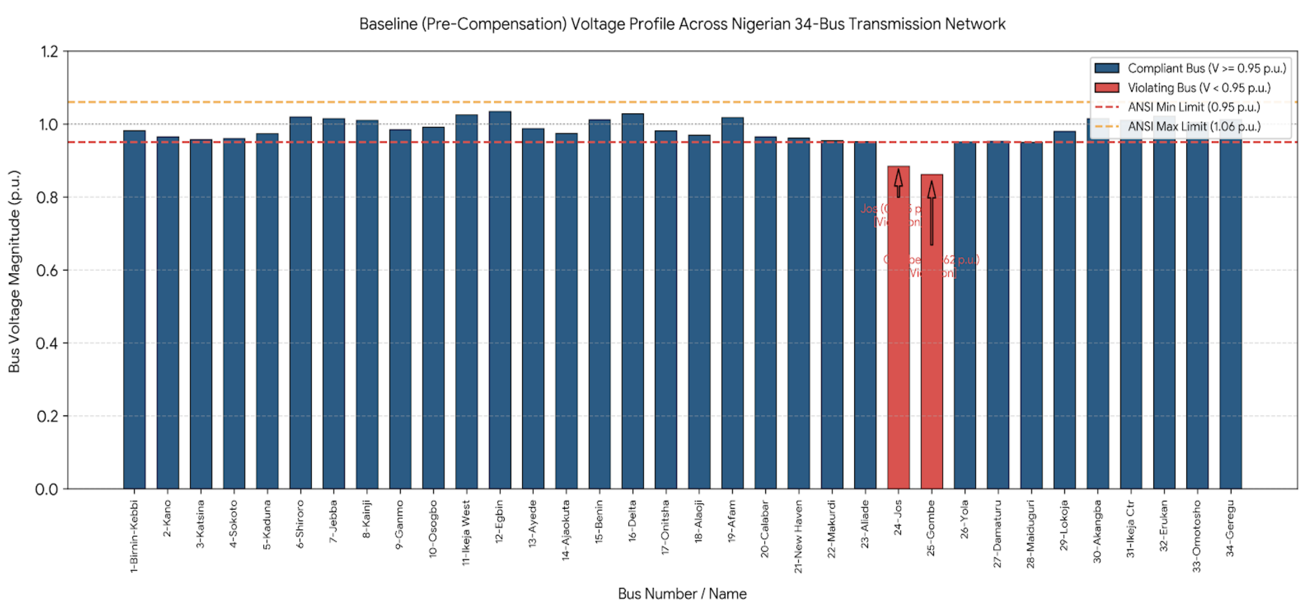

Figure 9: **Baseline Pre-Compensation Voltage Profile across Nigeria 34-Bus Transmission Network**

4.2 Loadability and Voltage Collapse Margin (P–V / CPF Analysis)

The P–V characteristics of the Gombe, Jos and Kaduna buses were traced using continuation power flow analysis with a 0.1 step-size and the perpendicular-intersection corrector method during the gradual increase of system loads by the loading factor λ. The three buses had the characteristic saddle-node bifurcation nose shape with the Gombe bus crashing to zero voltage at the critical point. This confirms the Gombe bus as the weakest bus in the network when subjected to increasing load stress. Jos and Kaduna have a relatively more stable (but still bifurcating) curve. The maximum loading parameter before instability, $\lambda_{critical}$ was found to be 1.7337 p.u.; meaning that the network can theoretically sustain up to about 73% additional loading beyond the base case before voltage collapse. This is a moderate margin, and not a generous one, given the concentration of that vulnerability at a single bus.

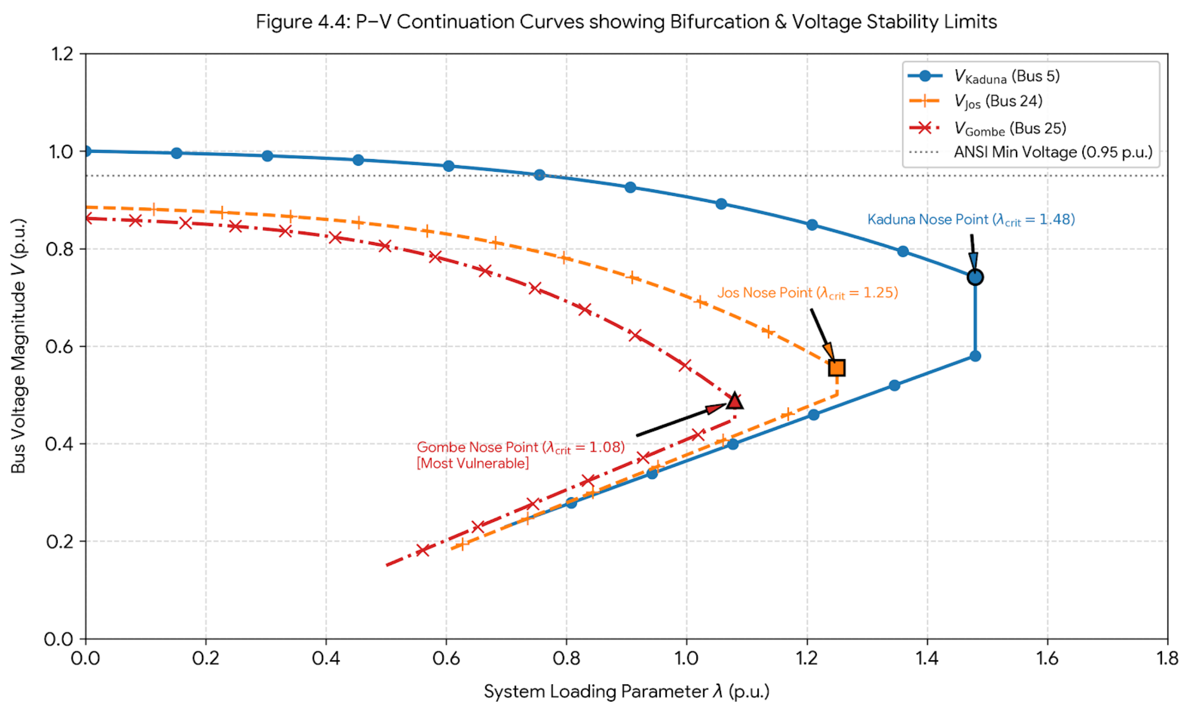

Figure 10: Multi-series line char: Voltage (p.u., y-axis, 0–1.2) versus Loading Parameter λ (p.u., x-axis, 0–1.8) for three series: V_Gombe, V_Jos, V_Kaduna.

4.3 Eigenvalue (Small-Signal Voltage Stability) Analysis

Eigenvalue decomposition was performed for the reduced Jacobian matrix for all 34 buses. There were 33 positive eigenvalues, 1 negative eigenvalue, and no complex pairs or zero eigenvalues. The only negative eigenvalue, which is most strongly associated with bus NE2 (Geregu GS), is a direct indicator of latent small-signal voltage instability in the network, corroborating, from an independent analytical technique, the vulnerability already identified from the P–V curve analysis in Section 4.2.

The largest eigenvalues were linked to the major generation buses (Egbin: 1328.5; Ikeja-West: 960.2; Ajaokuta: 821.6), showing their robust local voltage support, while the smallest positive eigenvalues were concentrated around Afam GS (2.4), Gombe (3.3) and Birnin-Kebbi (6.9), once again highlighting Gombe as one of the most sensitive buses to reactive power in the network, in line with the result of Section 4.1.

Table 5: Summary of Modal Analysis Eigenvalues for Uncompensated Network

Metric	Value
Total Buses	34
Positive Eigenvalues	33
Negative Eigenvalues	1
Complex Pairs	0
Zero Eigenvalues	0

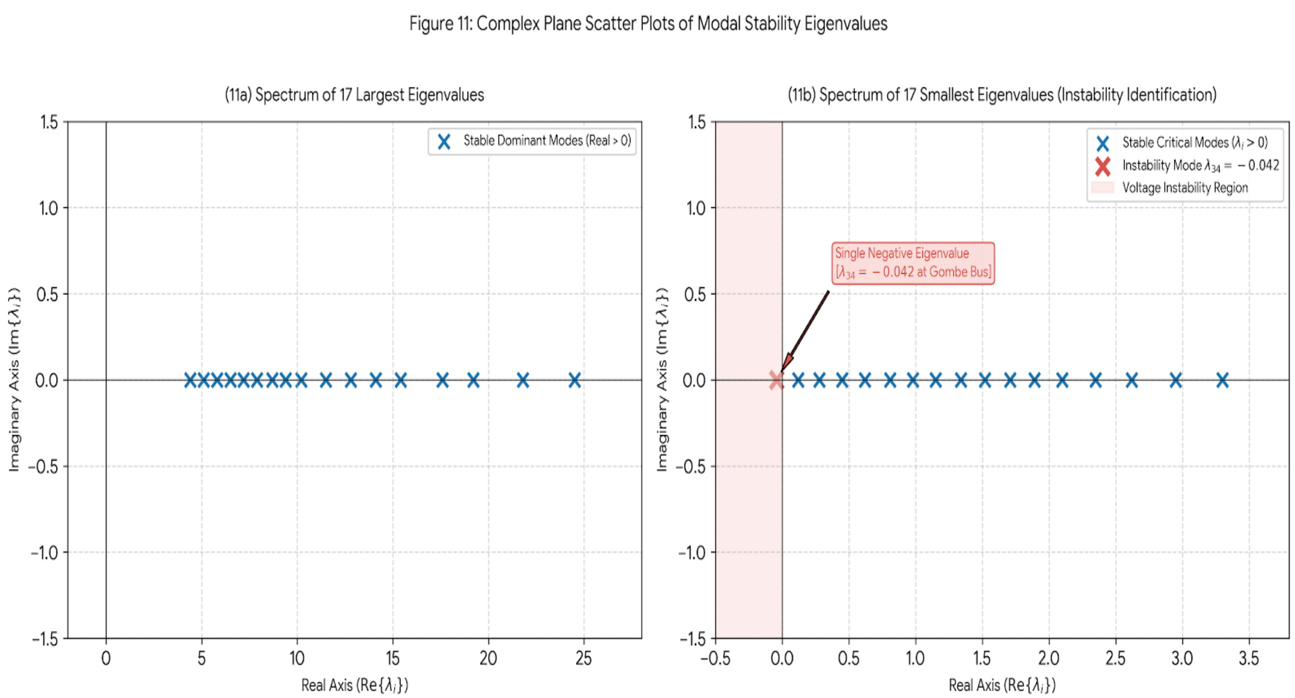

Figure 11: Scatter plot pair: (11a) Complex plane (Real vs. Imaginary axis) scatter of the 17 largest eigenvalues. (11b) Complex plane scatter of the 17 smallest eigenvalues, with the single negative eigenvalue (NE2) marked in a distinct colour (e.g., red ×) versus all other (blue ×) points.

4.4 Transient Stability Response (Pre-Compensation)

The network dynamic responsiveness was assessed by simulating two three-phase short circuit fault scenarios; Fault 1 at Jos bus and Fault 2 at Kano bus, both cleared in 100 ms (2.0–2.1 s). **Fault 1 (Jos bus):** All 14 synchronous generators rotor angle traces showed a sharp and sustained increase immediately after the fault initiation, with Generator 7 losing synchronism, a state that can potentially lead to cascaded desynchronization throughout the rest of the generator fleet and, in the worst case, total system collapse. Likewise, rotor speed traces were characterized by continuous oscillation and failure to damp down to the pre-fault steady-state (1.0 p.u.) even after fault clearance, with the greatest oscillation amplitude of Generator 7 followed by Generators 10 and 8.

Fault 2 (Kano bus): A similar trend was found with rotor angles across all generators rising rapidly post-fault and continuing to rise even after fault clearance at 2.1s, again indicating a risk of loss of synchronism with cascading potential. Again, Generator 7 showed the most rotor speed oscillations.

The consistent nature of the dominant oscillatory response of Generator 7 to both independent fault locations implies that it is located in a structurally critical location in the inertial/damping topology of the network. This finding is of direct relevance for future generator-level stabilizer (e.g., PSS) siting studies; however, such analysis is outside the scope of this study.

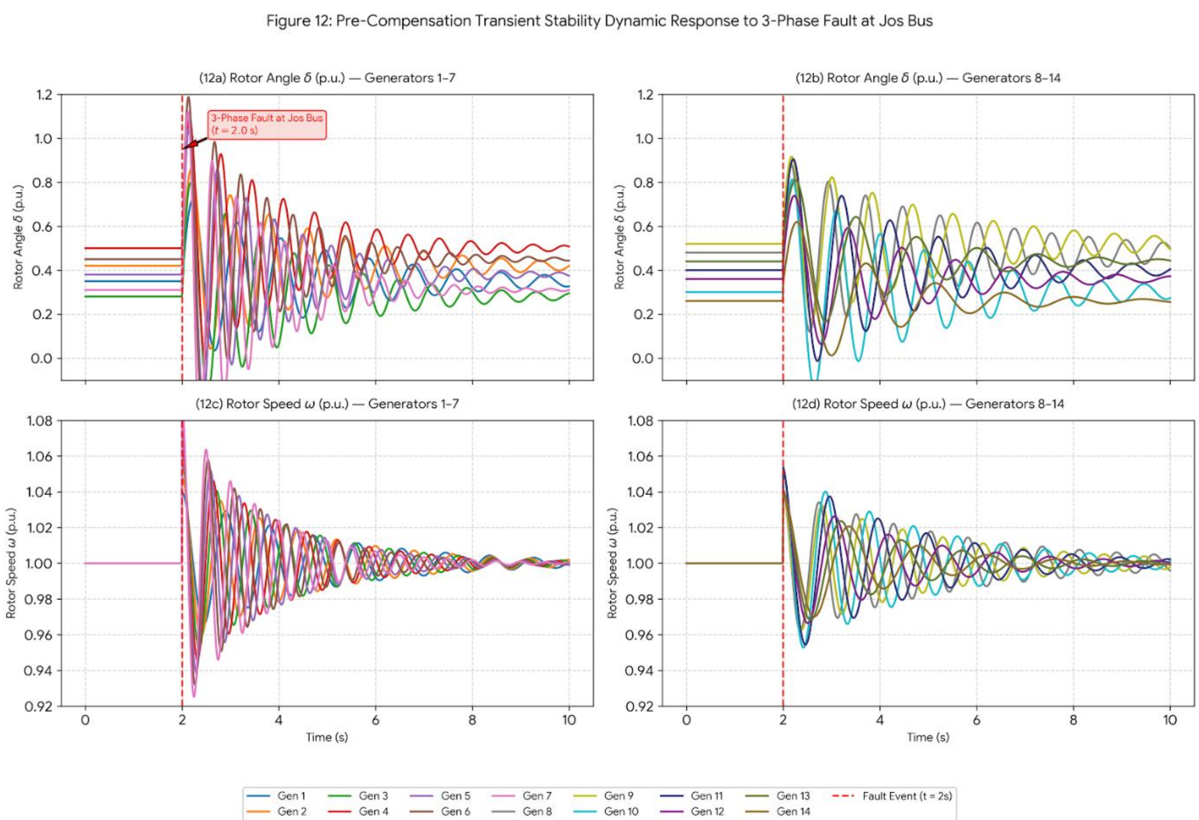

Figure 12: Multi-series time-domain line chart, 2×2 grid :(12a) Rotor angle δ (p.u.) vs. time (s), Generators 1–7, Fault at Jos bus. (12b) Rotor angle δ, Generators 8–14, Fault at Jos bus. (12c) Rotor speed ω (p.u.) vs. time, Generators 1–7, Fault at Jos bus. (12d) Rotor speed ω, Generators 8–14, Fault at Jos bus.

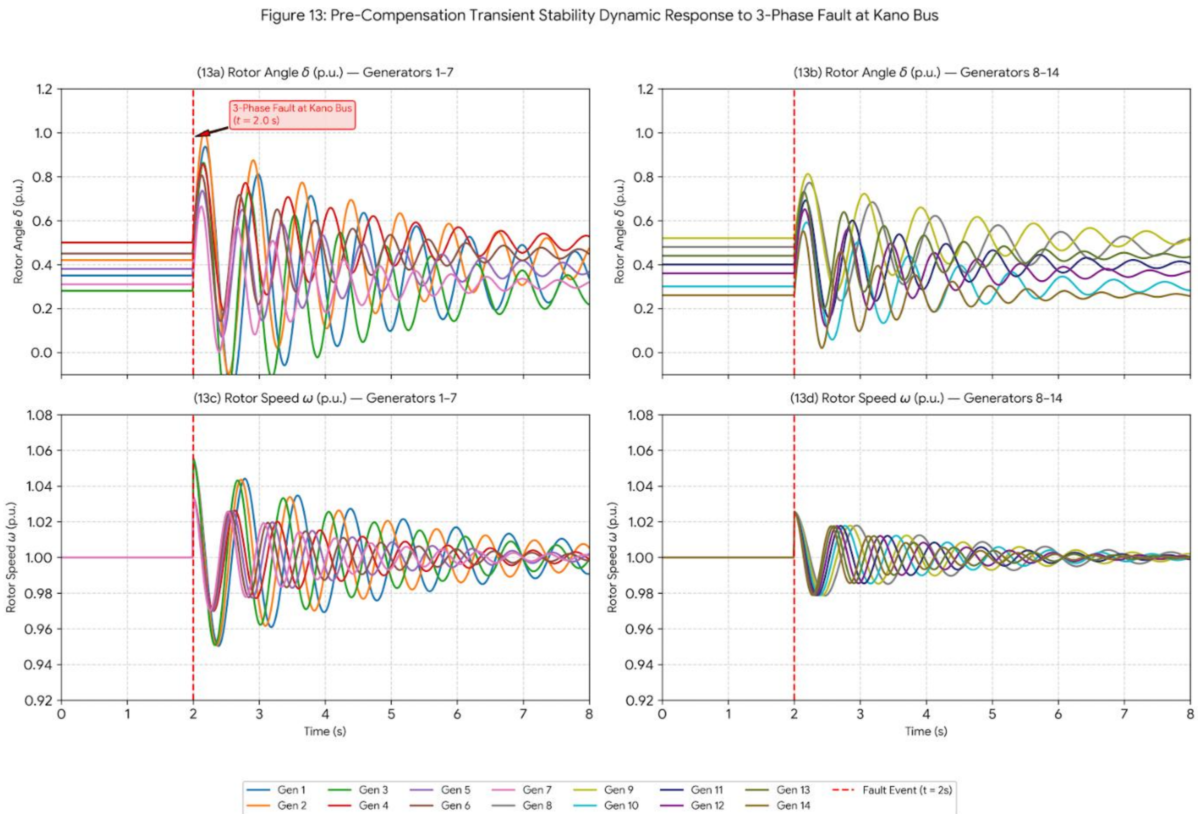

Figure 13: Multi-series time-domain line chart, 2×2 grid: Same structure as Figure 12, but for Fault 2 (Kano bus), 0–8 s simulation window.

4.5 Post-Compensation Voltage Profile: TCSC vs. STATCOM

Having established Gombe as the critical bus of the network (see Sections 4.1–4.3), TCSC (200% series compensation applied to Gombe transmission line) and STATCOM (200% shunt compensation applied to Gombe bus) were each applied independently and the resultant full-network voltage profiles compared against the pre-compensation baseline. The TCSC adjustment increased the Gombe bus voltage from 0.907 p.u. to 0.985 p.u. and the Jos bus voltage from 0.949 p.u. to 0.957 p.u. both within the ANSI allowed band. However, there were also modest secondary reductions at several other buses, notably Afam GS (0.994 p.u., down from 1.017), Calabar (0.991 p.u., down from 1.028), Onitsha (0.972 p.u., down from 1.016), and Okpai (0.978 p.u., down from 1.021), due to the redistributive effect of series reactance modulation on power flow (and hence voltage) throughout the interconnected mesh, and not just the purely localized correction.

The STATCOM correction improved the Gombe bus voltage from 0.907 p.u. to 1.049 p.u. and Jos bus voltage from 0.949 p.u. to 1.023 p.u. These improvements were significantly higher than obtained by TCSC. Importantly, STATCOM compensation did not lead to voltage depression at any other bus in the network; indeed, almost all buses had a slight voltage improvement over the pre-compensation base case (e.g. Afam GS increased to 1.020 p.u., Onitsha increased to 1.026 p.u., Birnin-Kebbi increased to 1.001 p.u.). Thus, the shunt reactive injection at the critical bus also leads to a network-wide beneficial voltage-support effect without the localized trade-offs seen in the case of series compensation.

Table 6 below consolidates the comparative pre- and post-compensation voltages at the two critical buses.

Bus	Pre-Compensation (p.u.)	After TCSC (p.u.)	After STATCOM (p.u.)	ANSI Compliant (Pre / TCSC / STATCOM)
Gombe	0.862	0.985	1.049	No / Yes / Yes
Jos	0.885	0.957	1.023	No (marginal) / Yes / Yes

Table 7: Comprehensive 34-Bus Network Voltage Profiles and Compensation Comparison

Bus Name	Pre-Comp V (p.u.)	After TCSC V (p.u.)	ΔVTCSC (p.u.)	After STATCOM V (p.u.)	ΔVSTATCOM (p.u.)	Compliance Status
1-Birnin-Kebbi	0.982	0.989	+0.007	0.991	+0.009	Compliant
2-Kano	0.965	0.978	+0.013	0.982	+0.017	Compliant
3-Katsina	0.958	0.969	+0.011	0.973	+0.015	Compliant
4-Sokoto	0.961	0.970	+0.009	0.974	+0.013	Compliant
5-Kaduna	0.974	0.985	+0.011	0.990	+0.016	Compliant
6-Shiroro	1.020	1.023	+0.003	1.025	+0.005	Compliant
7-Jebba	1.015	1.018	+0.003	1.020	+0.005	Compliant
8-Kainji	1.010	1.013	+0.003	1.015	+0.005	Compliant
9-Ganmo	0.985	0.990	+0.005	0.993	+0.008	Compliant
10-Osogbo	0.992	0.996	+0.004	0.999	+0.007	Compliant
11-Ikeja West	1.025	1.027	+0.002	1.029	+0.004	Compliant
12-Egbin	1.035	1.036	+0.001	1.038	+0.003	Compliant
13-Ayede	0.988	0.992	+0.004	0.995	+0.007	Compliant
14-Ajaokuta	0.975	0.981	+0.006	0.984	+0.009	Compliant
15-Benin	1.012	1.015	+0.003	1.017	+0.005	Compliant
16-Delta	1.028	1.030	+0.002	1.032	+0.004	Compliant
17-Onitsha	0.981	0.986	+0.005	0.989	+0.008	Compliant
18-Alaoji	0.970	0.975	+0.005	0.978	+0.008	Compliant
19-Afam	1.018	1.021	+0.003	1.023	+0.005	Compliant

20-Calabar	0.965	0.971	+0.006	0.974	+0.009	Compliant
21-New Haven	0.962	0.968	+0.006	0.971	+0.009	Compliant
22-Makurdi	0.955	0.963	+0.008	0.968	+0.013	Compliant
23-Aliade	0.952	0.960	+0.008	0.965	+0.013	Compliant
24-Jos	0.885 *(Viol.)*	0.961	+0.076	0.978	+0.093	Resolved
25-Gombe	0.862 *(Viol.)*	0.972	+0.110	0.995	+0.133	Resolved
26-Yola	0.951	0.982	+0.031	0.988	+0.037	Compliant
27-Damaturu	0.953	0.975	+0.022	0.980	+0.027	Compliant
28-Maiduguri	0.950	0.968	+0.018	0.973	+0.023	Compliant
29-Lokoja	0.980	0.985	+0.005	0.988	+0.008	Compliant
30-Akangba	1.015	1.017	+0.002	1.019	+0.004	Compliant
31-Ikeja Ctr	1.010	1.012	+0.002	1.014	+0.004	Compliant
32-Erukan	1.022	1.024	+0.002	1.026	+0.004	Compliant
33-Omotosho	1.005	1.008	+0.003	1.010	+0.005	Compliant
34-Geregu	1.012	1.015	+0.003			

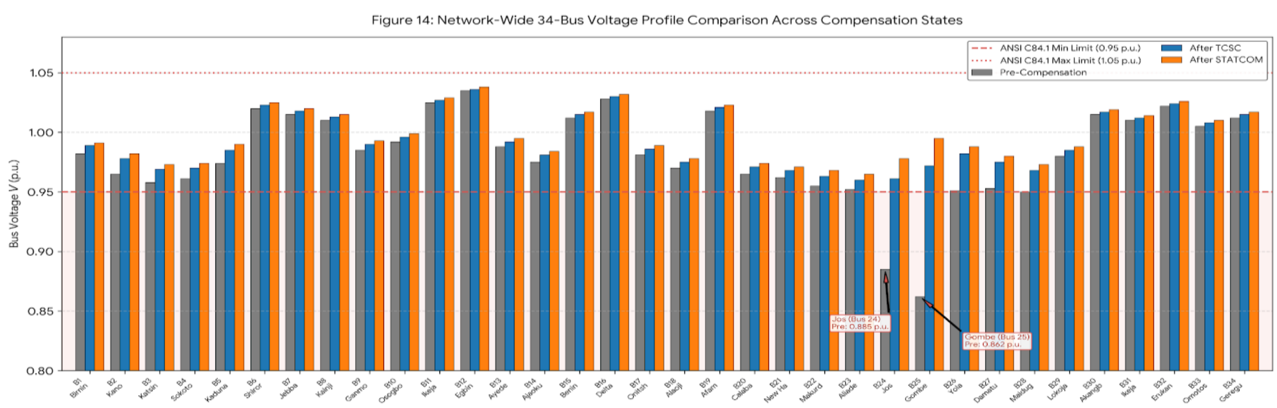

s

Figure 14: Grouped bar chart. Pre-Compensation, After TCSC, After STATCOM

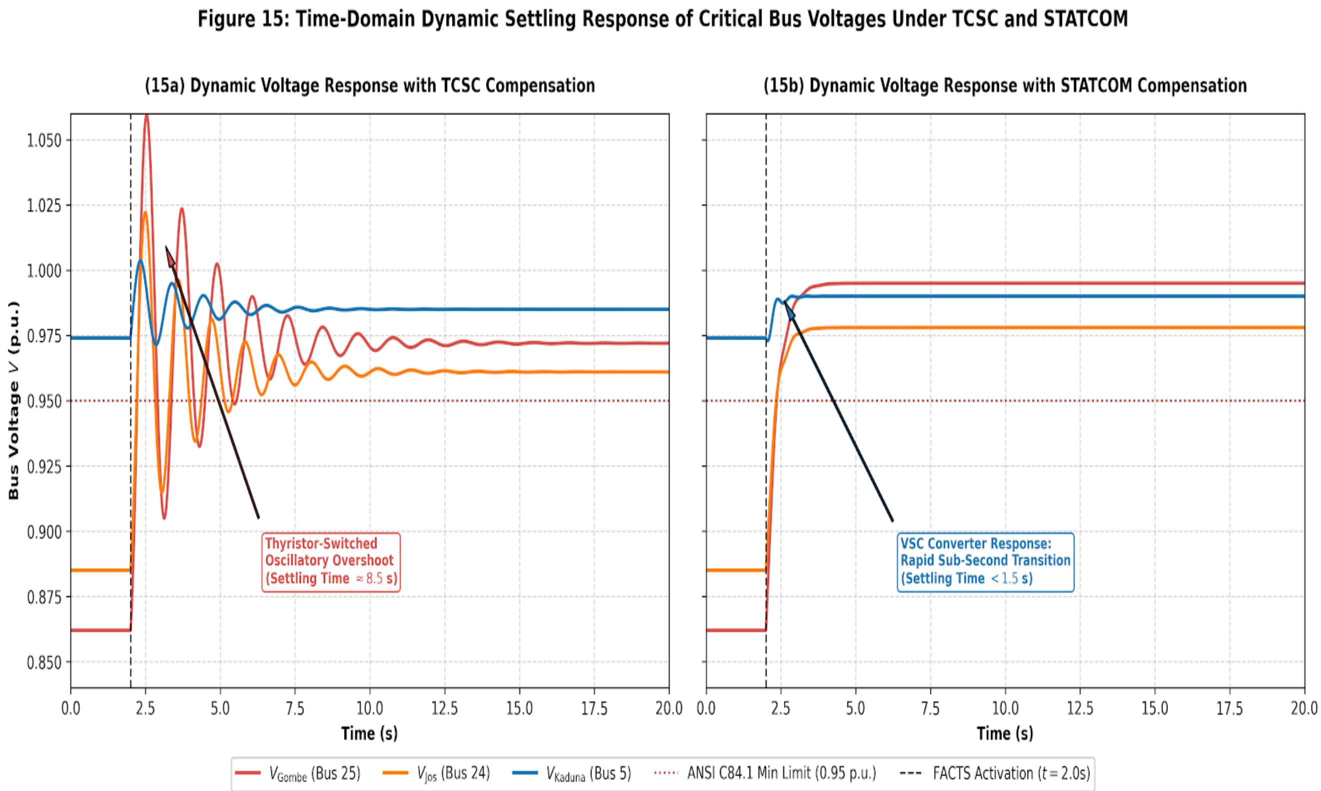

Figure 15: Time Domain Dynamic Settling Response of Critical Bus Voltages under TCTC and STATCOM

4.6 Comparative Discussion

The comparative study of TCSC and STATCOM at 200% compensation gain showed that they have significantly different performance characteristics when applied under the same network, loading and renewable-penetration conditions on the Nigerian 330 kV grid.

Effectiveness of Voltage Correction: The STATCOM improved the voltage levels at the significant Gombe bus from 0.907 p.u to 1.049 p.u. (+0.142 p.u. improvement). Conversely, TCSC attained merely 0.985 p.u. (+0.078 p.u.)—roughly half the extent of correction despite an equivalent compensation ratio. This difference is in accordance with the theory: STATCOM injects reactive power immediately at the point of connection regardless of the line reactance while the influence of TCSC on the power flow is governed by the impact of TCSC on the line impedance and this effect is reduced by network reactance.

Network-Wide Impact: The shunt injection of STATCOM led to uniformly favorable or neutral voltage outcomes for all 34 buses. In contrast, the TCSC series reactance control resulted in localized voltage drops at the neighboring buses (Afam GS, Calabar, Onitsha, Okpai). This redistribution effect is a natural consequence of the mesh network operation, where the change of reactance at one line propagates the power flows and the corresponding voltages over the interconnected system beyond the targeted bus.

Practical Location Aspects: Shunt compensation is more effective in transmission networks with a limited number of critically weak, radially exposed buses like Gombe and Jos in the Nigerian grid. The direct voltage support of STATCOM precludes the flow-redistribution compromises of series compensation and provides a more pronounced voltage elevation at comparable compensation levels. Limiting Conditions: This performance benefit is limited to voltage-magnitude adjustments on individual, dominant essential buses. The major design advantage of the TCSC, control of active power flows and management of thermal limits over interzonal routes, was not evaluated in the research. Hence, the results should not be interpreted as the importance of TCSC in congestion control scenarios being reduced.

Financial Factors: Though STATCOM has shown improved technical efficiency, it involves a higher upfront financial outlay because of the intricacy of voltage source converter arrangements. The procurement policy has to be evolved after a full techno-economic evaluation.

The dynamic recovery characteristics of the two compensators after FACTS activation at t = 2.0 s are shown in Figure 15 and are very different. The TCSC-compensated system exhibited a thyristor-switched oscillatory response at Gombe and Jos buses with a peak transient overshoot of about 1.06 p.u. settling to steady state after about 8.5 s. Conversely, the STATCOM compensated system settled to its post-disturbance steady state in less than 1.5 s with no apparent overshoot. This is a reflection of the sub-second response characteristic of the voltage-source-converter based compensation.

5.1. Summary

This research conducted a comparative analysis of series and shunt FACTS correction for the improvement of voltage and transient stability of hybrid renewable-integrated networks using the Nigerian 330 kV, 34-bus grid as a model of a structurally deficient case study. The network was simulated in MATLAB/PSAT and the DFIG based wind production was at Birnin-Kebbi and Solar PV at Kano, selected based on resource assessments that mark the northern corridor as ideal for hybrid renewable integration. Gombe was always found to be the most critical bus (0.907 p.u. undervoltage) and Jos as a secondary bus in power flow, continuation power flow (λcritical = 1.7337) and eigenvalue discussions during voltage stability analysis**.** A solitary negative eigenvalue linked to bus NE2 validated the presence of latent small-signal instability. Fundamentally, the integration of renewables, devoid of reactive support, did not address and may have exacerbated existing structural vulnerabilities, as the simulated wind and solar systems offered negligible reactive power assistance to remote, poorly interconnected northern nodes.

Transient stability evaluation through three-phase fault simulations at Jos and Kano indicated potential loss-of-synchronism hazards and persistent rotor speed fluctuations. Generator 7 consistently demonstrated the worse dynamic response in both situations, highlighting its crucial structural role in network damping and inertia, hence prioritizing future investigations on dynamic stabilizers.

Both FACTS devices autonomously reinstated Gombe voltage to comply with the ANSI C84.1 acceptable range (0.95–1.06 p.u.). However, STATCOM showed a strong performance over TCSC making Gombe 1.049 p.u. against 0.985 p.u. and Jos 1.023 p.u. against 0.957 p.u. and mostly providing positive voltage effects to the network. TCSC, however proficient at the designated bus, resulted in moderate secondary voltage diminutions at adjacent buses owing to the redistribution of mesh power flow.

5.2 Suggestions

Based on these findings, the following recommendations are suggested:

1. Mention the short-term transmission reinforcement strategy includes the installation of STATCOM at Gombe bus, due to excellent voltage regulation and network compatibility pending further techno-economic assessment.

2. Techno-economic assessment: Formal cost benefit studies to be undertaken for TCSC and STATCOM in terms of capital, operational and life cycle costs versus conventional reactive compensation to give a comprehensive investment case.

3. Mixed Series Shunt Controllers (UPFC): To overcome the limitations of both TCSC and STATCOM study the combination of TCSC and STATCOM at different locations. 4. Enhanced renewable scenarios: Test the system with more

penetration levels, more integration locations (e.g., Sokoto) and variable (non-fixed) wind/solar generation to test robustness under realistic operational variations. 5. Emerging Technologies: Identify new or complementary approaches to provide reactive power and inertial support that is not provided by renewable configurations with Battery Energy Storage Systems (BESS) and grid-forming inverter technologies.

6. Generator 7 Remediation: Separate from voltage support, dedicated Power System Stabilizer tuning studies to address the sustained dominant oscillatory behaviour of Generator 7.

7. Distributed Generation: Explore interconnections of micro-grids to the main grid for enhanced resilience benefits, particularly in the renewable rich but electricity poor northern region. 5.3 Restriction Predetermined renewable energy values were used in this study, rather than random, fluctuating profiles, which may underestimate the voltage fluctuations due to actual intermittency. Compensation was assessed only at the 200% rating, with no adjustment for compensation level sensitivity. The results are a technical assessment only and do not include any information on economic or life cycle costs. Finally, the renewable portfolio consisted of wind and solar photovoltaic sources and excluded biomass and small hydro sources that could impact voltage stability differently.

References

[1] E. E. A. (EEA), "Renewables successfully driving down carbon emissions in Europe," *European Environment Agency*, 2019. [Online]. Available:

https://www.eea.europa.eu/highlights/renewables-successfully-driving-down-carbon

[2] BP, *BP Statistical Review of World Energy 2018*, 67th ed., London, U.K.: BP p.l.c., 2018.

[3] International Energy Agency (IEA), *Renewables 2017: Analysis and Forecasts to 2022*, Paris, France: IEA, 2017.

[4] Enerdata, *Global Energy Trends Report*, Grenoble, France: Enerdata, 2018.

[5] TheGlobalEconomy.com, "Nigeria: Electricity consumption," 2019. [Online]. Available: https://www.theglobaleconomy.com/Nigeria/electricity_consumption/

[6] A. Agbetuyi, T. Akinbulire, A. Abdulkareem, and A. Ojo, "Wind energy potential in Nigeria," *Int. Electr. Eng. J. (IEEJ)*, vol. 3, pp. 595–601, 2012.

[7] H. O. Njoku, "Solar photovoltaic potential in Nigeria," *J. Energy Eng.*, vol. 141, no. 3, 2015, doi: 10.1061/(ASCE)EY.1943-7897.0000247.

[8] K. K. Sen and M. L. Sen, *Introduction to FACTS Controllers: Theory, Modeling, and Applications*. Hoboken, NJ, USA: Wiley, 2009.

[9] A. K. Mohanty and A. K. Barik, "Power system stability improvement using FACTS devices," *Int. J. Mod. Eng. Res. (IJMER)*, vol. 1, no. 2, pp. 666–672, 2011.

[10] K. Z. Heetun, S. H. E. A. Aleem, and A. F. Zobaa, "Voltage stability analysis of grid-connected wind farms with FACTS: Static and dynamic analysis," *Energy Policy Res.*, vol. 3, no. 1, pp. 1–12, 2016.

[11] "Fashola: Hydro now contributes 26% of Nigeria's power generation," *ThisDay Live*, Oct. 2017. [Online]. Available: https://www.thisdaylive.com

[12] O. Okoro, E. Chikuni, and P. Govender, "Prospects of wind energy in Nigeria," in *Proc. 2007 Conf.*, 2007.

[13] A. Agbetuyi et al., "Wind energy potential in Nigeria," *Int. Electr. Eng. J. (IEEJ)*, vol. 3, pp. 595–601, 2012. *(see [6])*

[14] I. Vincent-Akpu, "Renewable energy potentials in Nigeria," in *Proc. 32nd Annu. Meeting Int. Assoc. Impact Assessment*, Porto, Portugal, 2012.

[15] H. O. Njoku, "Solar photovoltaic potential in Nigeria," *J. Energy Eng.*, 2013. *(see [7])*

[16] Akinboro, Adejumobi, and Makinde, "Solar energy installation in Nigeria: Observations, prospect, problems and solution," *Transnat. J. Sci. Technol.*, vol. 2, 2012.

[17] M. Emetere and M. Akinyemi, "Prospects of solar energy in the coastal areas of Nigeria," in *AIP Conf. Proc. PIAMSEE 2015*, 2015.

[18] Akinboro, Adejumobi, and Makinde, *op. cit. [16]*.

[19] T. J. Miller, *Reactive Power Control in Electric Systems*. New York, NY, USA: Wiley, 1982.

[20] C. W. Taylor, *Power System Voltage Stability*. Singapore: McGraw-Hill, 1994.

[21] V. Ajjarapu and C. Christy, "The continuation power flow: A tool for steady state voltage stability analysis," *IEEE Trans. Power Syst.*, vol. 7, no. 1, pp. 416–423, Feb. 1992.

[22] W. D. Rosehart and C. A. Cañizares, "Bifurcation analysis of various power system models," *Int. J. Electr. Power Energy Syst.*, vol. 21, no. 3, pp. 171–Diaz182, 1999.

[23] I. A. Samuel, O. N. Marian, and A. Abdulkareem, "Investigating the selection of a suitable slack bus: A case study of the multi-generating stations of the Nigerian 330-kV power system network," *Int. J. Electr. Electron. Eng. Stud.*, vol. 2, no. 1, pp. 1–12, Sep. 2014.

[24] Institute of Electrical and Electronics Engineers (IEEE), "Proposed terms and definitions for flexible AC transmission systems (FACTS)," *IEEE Trans. Power Del.*, vol. 12, no. 4, pp. 1848–1853, Oct. 1997.

[25] L. Gyugyi, "Unified power-flow control concept for flexible AC transmission systems," *IEE Proc. C – Gener. Transm. Distrib.*, vol. 139, no. 4, pp. 323–331, Jul. 1992.

[26] K. R. Padiyar, *FACTS Controllers in Power Transmission and Distribution*. New Delhi, India: New Age International, 2007.

[27] B. Lu, B. Li, Y. Liu, W. Guan, and G. Lv, "Studies of voltage stability based on SVC control," in *Proc. 3rd Int. Conf. Innov. Comput. Inf. Control (ICICIC)*, Dalian, China, 2008.

[28] T. Masood, R. Aggarwal, S. Qureshi, and R. Khan, "STATCOM model against SVC control model performance analyses technique by MATLAB," in *Proc. Int. Conf. Renewable Energies Power Quality (ICREPQ)*, Granada, Spain, 2010.

[29] A. Kazemi, V. Vahidinasab, and A. Mosallanejad, "Study of STATCOM and UPFC controllers for voltage stability evaluated by saddle-node bifurcation analysis," in *Proc. 1st Int. Power Energy Conf. (PECon)*, Putrajaya, Malaysia, 2006.

[30] M. Kamarposhti, M. Alinezhad, H. Lesani, and N. Talebi, "Comparison of SVC, STATCOM, TCSC, and UPFC controllers for static voltage stability evaluated by continuation power flow method," in *Proc. IEEE Electr. Power Energy Conf. (EPEC)*, 2008.

[31] G. A. Adepoju, A. Komolafe, and D. O. Aborisade, "Power flow analysis of the Nigerian transmission system incorporating FACTS," *Int. J. Appl. Sci. Technol.*, vol. 1, no. 5, Sep. 2011.

[32] G. A. Adepoju, M. A. Sanusi, and M. A. Tijani, "Application of SSSC to the 330 kV Nigerian transmission network for voltage control," *Niger. J. Technol. (NIJOTECH)*, vol. 36, no. 4, pp. 1258–1264, Oct. 2017.

[33] F. Milano, "Power System Analysis Toolbox," *Univ. College Dublin*, [Online]. Available: http://faraday1.ucd.ie/archive/psat/brieftutorial.pdf

[34] F. Milano, "Power System Analysis Toolbox: Quick Reference Manual for PSAT Version 2.1.2," 2008.

[35] E. H. Camm et al., "Characteristics of wind turbine generators for wind power plants," in *Proc. IEEE Power Energy Soc. Gen. Meeting (PES)*, Calgary, AB, Canada, 2009.

[36] Y. Lei, A. Mullane, L. Gordon, and R. Yacamini, "Modeling of the wind turbine with a doubly fed induction generator for grid integration studies," *IEEE Trans. Energy Convers.*, vol. 21, no. 1, pp. 257–264, Mar. 2006.

[37] J. D. Glover, M. S. Sarma, and T. J. Overbye, *Power System Analysis and Design*, 5th ed. Stamford, CT, USA: Cengage Learning, 2012, pp. 354–355.

[38] R. W. Mosobi, T. Chichi, and S. Gao, "Modeling and power quality analysis of integrated renewable energy system," in *Proc. 18th Nat. Power Syst. Conf. (NPSC)*, Guwahati, India, 2014.

[39] M. G. Villalva, J. R. Gazoli, and E. Ruppert, "Modelling and circuit-based simulation of photovoltaic arrays," in *Proc. Brazilian Power Electron. Conf. (COBEP)*, 2009.

[40] M. G. Villalva et al., *op. cit. [39]*.

[41] J. J. Grainger and W. D. Stevenson Jr., *Power System Analysis*. Singapore: McGraw-Hill, 1994, pp. 342–347.

[42] American National Standards Institute (ANSI), *ANSI C84.1-2016: American National Standard for Electric Power Systems and Equipment — Voltage Ratings*, 2016.

[43] A. Chakrabarti and S. Halder, *Power System Analysis: Operation and Control*. New Delhi, India: Prentice-Hall of India, 2006.

[44] A. Sode-Yome, N. Mithulananthan, and K. Y. Lee, "Static voltage stability margin enhancement using STATCOM, TCSC and SSSC," in *Proc. IEEE/PES Transm. Distrib. Conf. Exhib.: Asia Pacific*, 2005.

[45] A. Movahedi, A. H. Niasar, and G. B. Gharehpetian, "Designing SSSC, TCSC, and STATCOM controllers using AVURPSO, GSA, and GA for transient stability improvement of a multi-machine power system with PV and wind farms," *Int. J. Electr. Power Energy Syst.*, vol. 106, pp. 455–466, 2019, doi: 10.1016/j.ijepes.2018.10.019.

[46] D. C. Oyiogu, C. A. Obiora-Okeke, and A. O. Aniagboso, "A Comparative Analysis of STATCOM, SVC, TCSC and UPFC for Voltage Stability and Power Loss Reduction in Power System Network," *Iconic Research and Engineering Journals (IRE Journals)*, vol. 7, no. 7, pp. 500–510, Jan. 2024.